Available online at www.sciencedirect.com
SCIENCE DIRECT®
Journal of Solid State Chemistry 177 (2004) 1372–1381
JOURNAL OF SOLID STATE CHEMISTRY
http://elsevier.com/locate/jssc

Low-temperature synthesis and microstructural control of titania nano-particles

Y. Li,* T.J. White, and S.H. Lim

Centre for Advanced Research of Ecomaterials, Institute of Environmental Science and Technology, Nanyang Technological University, Innocation Centre (NTU), Blk 2, Unit 237, 18 Nanyang Drive, Singapore 637723, Singapore

Received 24 July 2003; received in revised form 6 November 2003; accepted 23 November 2003

Abstract

Nanocrystalline titania powders were synthesized at low temperature ($\leqslant 100^{\circ}C$) by a sol–gel method that achieved fine control of particle size and polymorph fraction. X-ray diffraction (XRD), transmission electron microscopy (TEM) and UV–Vis spectroscopy were used to characterize the phase assemblages, crystal size and band gap of the powders. It was demonstrated that larger, well-ordered titania crystals can be obtained by increasing aging temperature and time. These processing parameters can be adjusted to select specific polymorphs from the gel precursors with particular size and shape. The quantum size effect was observed in the size-controlled nanocrystalline titania particles, leading to a blue shift in UV absorption with decreasing in particle size. The anatase to rutile transformation, which may proceed with brookite as a transition phase, is dependent on both particle size and surface structure of the nascent crystals.

Keywords: Titania; Nanoparticles; Microstructure control; Sol–gel

1. Introduction

Titania semiconductor photocatalysts have been widely studied for air and water purification due to their powerful oxidation strength, high photostability and nontoxicity [1,2]. The principles of photoexcitation are well understood. Ultraviolet and visible light (2.5–4.0 eV) match the band gap of titania to yield electron–hole pairs. Photocatalytic efficiency depends on the ratio of the surface charge carrier transfer rate to the electron–hole recombination rate. Properties influencing the photocatalytic activity of titania particles have been reported to include surface area, crystallinity, crystallite size and crystal structure [1,3]. Consequently, the manipulation of microstructure, especially for nanocrystalline powders, is essential to optimize photocatalytic efficiency. For titania, the three common polymorphs among others are anatase, rutile and brookite. It is generally accepted that anatase is the most active photocatalyst, and that a combination of high crystallinity and large specific surface area improves photocatalytic performance [4,5]. These physical properties are controlled by the preparation method.

Of the three naturally occurring forms of titania, anatase and brookite are thermodynamically metastable with respect to rutile. All three crystal structures consist of TiO_6 octahedra connected variously by corners and edges, as presented in Fig. 1. In rutile, two opposing edges of each octahedra are shared to form linear chains along [001]. These TiO_6 chains are linked to each other through corner connection. Anatase has no corner sharing, but has four edges shared per octahedron. The anatase structure can be viewed as zigzag chains of octahedra, linked to each other through shared edges. The density of rutile and anatase is 4.26 and 3.84 g/cm^3 respectively [6]. In brookite, the octahedra share both edges and corners, forming an orthorhombic structure with a density of 4.11 g/cm^3.

The sol–gel method, which involves the hydrolysis and condensation of alkoxide precursors, is a reliable method to synthesize ultra-fine metallic oxides and has been widely employed for the preparation of titanium dioxide nanocrystals [7,8]. Depending on the respective kinetics of the two reactions, oxo-polymers can be obtained from titanium alkoxides in homogeneous gels

*Corresponding author. Fax: +65-67921291.
E-mail address: yli@ntu.edu.sg (Y. Li).

0022-4596/$ - see front matter © 2003 Elsevier Inc. All rights reserved.
doi:10.1016/j.jssc.2003.11.016

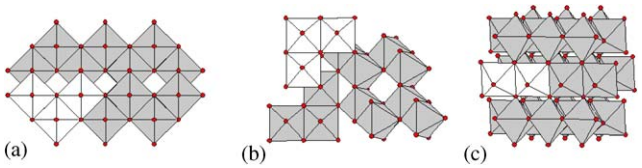

Fig. 1. Crystal structure of (a) anatase, (b) brookite and (c) rutile showing the TiO_6 octahedral arrangement and emphasizing their fundamental octahedral cluster (unshaded octahedral).

or fine precipitates. The overall polycondensation reaction is a complex process and depends on many parameters. The propensity for titanium alkoxides to rapidly hydrolyze makes their sol–gel transformation difficult to control [9], and consequently variations in preparative route can yield very different products [10,11]. Detailed and systematic studies of these effects are rarely reported, and contrary results are readily found in Refs. [3,12,13]. Some researchers investigated the formation of TiO_2 colloids via the hydrolysis and condensation of alkoxides under a large excess of water [14,15]. However, much ambiguity remains concerning the evolution and fine control of titania nanocrystals during the transition from titanium alkoxide precursor to the oxide.

The widely used processing routes to fabricate titania, such as sol–gel processing [16,17], cathodic electrodeposition [18] and so on, usually require subsequent thermal treatment at temperatures $>400°C$ to crystallize the amorphous titania, a procedure accompanied by grain coarsening and a reduction in surface area. This represents a technological limitation as heat-treatment at these temperatures prevents the immobilization of titania nanocrystals on some common or potential substrates, such as polymers and metals with low melting points. This restricts the fabrication of catalytic composites, electrodes and other devices. Therefore, the development of low-temperature synthesis of nanocrystalline titania is essential for its implementation across a wider range of applications.

In this work, nanocrystalline titania powders with controlled-size and polymorph composition were synthesized at low temperatures ($<100°C$). The influence of processing parameters on the structure, phase stability and photocatalytic properties of nanocrystalline titania are systematized. Unique observations concerning the stability fields and crystallization of titania polytypes are reported.

2. Experimental methods

2.1. Powder preparation

Tetrabutyl titanate ($Ti(O–Bu)_4$) was hydrolyzed using anhydrous ethanol (EtOH) as the solvent and various water concentrations. Hydrochloric acid (HCl) was added as a catalyst. These detailed procedures have been reported earlier [19]. Aging of the dry and wet gel, as well as water concentrations were varied systematically to study their influence on the products. The wet-gel was dried at 60°C using a vacuum pump for 5 h. The dry gel was then heat treated at different temperatures.

2.2. XRD

Powder X-ray diffraction (XRD) was used for identification of crystalline phases and estimation of crystallite size. The XRD patterns were recorded in the range of $2\Theta = 10-140°$ by step scanning, using 2θ increments of 0.02° and a fixed counting time of 5 s/step, with a Siemens diffractometer (D5005) employing Cu$K\alpha$ radiation. Structure refinements were performed by a Rietveld method using a fundamental parameters procedure [20]. In this manner, the average crystal size and polytype composition, as well as the unit cell parameters, were obtained.

2.3. TEM

The samples were suspended in distilled water, dispersed ultrasonically to separate individual particles, and one or two drops of the suspension deposited onto holey carbon coated copper grids. High resolution electron microscopic (HREM) and bright field images were collected using a JEOL JEM-3010 transmission electron microscope operated at 300 kV.

2.4. DSC/TGA

The dried titania powders were subjected to thermo gravimetric (TGA) and differential scanning calorimetric (DSC) analysis (NETZSCH STA 409 system) to determine the temperatures of possible decomposition and phase transformations. The samples were heated at the rate of 10°C/min to 1200°C with N_2 as the balance gas and air as the sample gas.

2.5. BET

The Brunauer–Emmett–Teller (BET) surface area was determined using a Micromeritics ASAP 2010 nitrogen adsorption apparatus. The samples were dried in a flow of inert gas (helium) at 250°C and the surface area of the samples estimated by N_2 chemisorption.

2.6. UV–Vis spectrometer

Powder samples used for the absorption studies were introduced to a Jasco V-550UV–Vis spectrophotometer.

The quantum size effect was estimated directly from UV diffuse reflectance spectra.

3. Results

3.1. Effects of aging dry gel at low temperature

The as-prepared dry gel was aged at 100°C in air for 12 h. The DSC/TGA curves of the as-prepared and aged dry gel are distinct (Fig. 2). The as-prepared dry gel undergoes endothermic dehydration in the temperature range 80–150°C [21]. Exothermic peaks, localized at 246°C and 430°C, reflect the processes of oxidation of the organic residuals and increasing crystallization of the anatase structure [22,23]. The weight-loss in the aged dry gel, which is mainly due to the removal of water and organic components from the structure, is less than that for the as-prepared dry gel. There is only one prominent endothermic peak at ~118°C in its DSC curve. The exothermic peaks were less pronounced than those of the as-prepared dry gel. This may be due to evaporation of some organic components during aging at 100°C for 12 h.

The XRD patterns of the as-prepared and aged dry gel show that substantial crystallization of anatase took place in the latter, illustrating that aging is not only helpful for organics removal, but also for the atomic diffusion and crystallization of anatase (Fig. 3).

Selected-area electron diffraction (SAED) and HRTEM studies confirmed that the crystallinity was less developed in the as-prepared sample as compared to the aged sample. Fig. 4 shows a HRTEM image of the aged TiO_2 sample. Most of the TiO_2 grains in this sample have a size of about 6–10 nm, in reasonable agreement with the XRD results (8 nm). The diffraction pattern clearly indicates a crystalline structure for this sample. All the diffraction rings can be indexed using anatase. The SAED patterns of the samples calcined at 200°C, 300°C, and 400°C are similar to that shown in Fig. 4.

To improve our understanding of the phase stability of nano-sized titania, both the dry and aged gels were sintered in air from 200°C to 800°C for 2 h. At lower temperatures (<500°C) Bragg reflections corresponding to anatase only were recognized. The peak widths gradually decrease with increasing temperature, indicating that the particle size of anatase increased slowly. It was found that the onset transformation temperature of anatase to rutile ($A \rightarrow R$) was different in the two gels. For the as-prepared dry gel, all reflections correspond to anatase below 500°C. Rutile began to appear at 600°C, and its proportion increased rapidly above that temperature. Only trace anatase remained after heat-treatment at 800°C for 2 h. As for the aged dry gel, $A \rightarrow R$ transformation commenced at 500°C, which is 100°C lower than in the as-prepared dry gel, and was complete at 800°C.

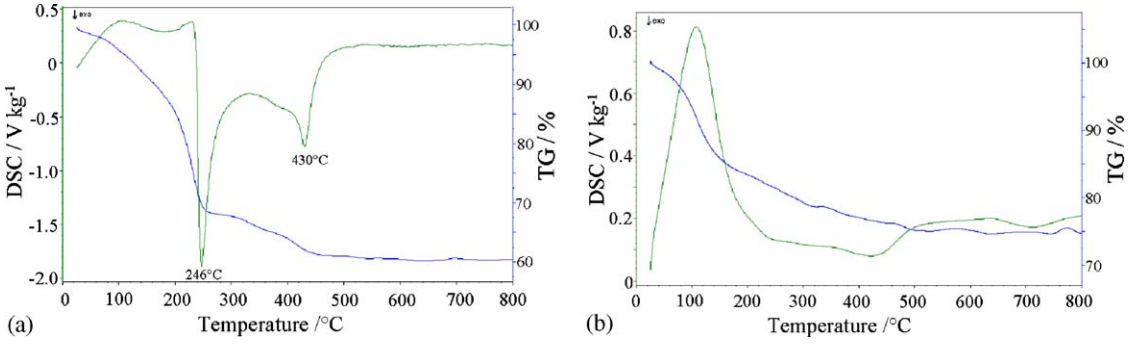

Fig. 2. DSC/TGA curves of titania nano-powders (a) as-prepared, (b) aged at 100°C for 12 h.

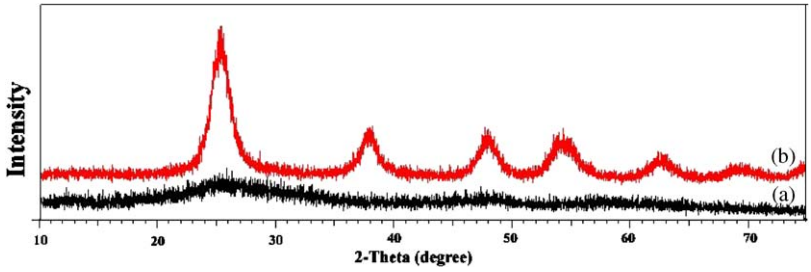

Fig. 3. XRD spectra of titania nano-powders (a) as-prepared, (b) aged at 100°C for 12 h.

XRD Rietveld refinement was performed using as starting models the structures determined earlier for rutile [24], brookite [25] and anatase [26]. The parameters refined were zero-point correction, unit cell parameters, scale factor, background and peak width, but atomic co-ordinates, occupancies and thermal parameters were fixed. Typical agreement is depicted in Fig. 5 and the overall results are summarized in Fig. 6. The particle diameter for the as-prepared product is <3 nm, with aging at 100°C for 12 h leading to an increase to 8 nm. Below 500°C, anatase crystals grew slowly because of the large activation energy for an atom to leave the matrix and attach itself to the growing phase at lower temperatures. At 500°C and above, the crystals in the as-prepared dry gel are slightly larger than in the aged gel, as for example, diameters of anatase at 500°C were 28 and 19 nm, respectively. However, the polymorph in the as-prepared gel was 100 wt% anatase at this temperature, while ~ 5 wt% rutile formed in the aged gel. Above 600°C, the particle sizes for both anatase and rutile increased rapidly due to the small activation energy for atom mobility at higher temperatures, but the particle size of rutile in the heat-treated aged-gel was much smaller than that in the as-prepared gel. In Fig. 6(c) the trend of unit cell parameters shows that a decreased with temperature while c increased, with the unit cell volume declining leading to a denser packing of the atoms.

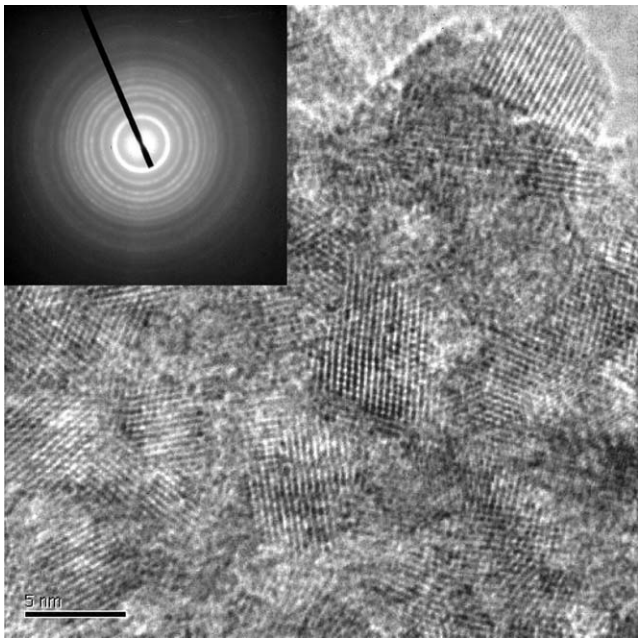

Fig. 4. SAEDP and HRTEM image of titania nano-powders aged at 100°C for 12 h.

The results of BET surface area analysis are in good agreement with the XRD and TEM results. The as-prepared powders possess a specific surface area of 248.3 m^2/g, while the aged titania has a value of 160 m^2/g. Heat-treatment reduced surface area rapidly, from 171.2 m^2/g at 300°C to 2 m^2/g at 700°C for the as-prepared dry gel.

The UV–Vis absorption band edge is a strong function of titania cluster size for diameters less than 10 nm, which can be attributed to the well-known quantum size effect for semiconductors [27]. Extrapolating the spectral curves to the long-wavelength side provides a measure of the band gap energy of the nanoparticles. The UV–Vis spectra of the aged titania are shown in Fig. 7. The absorption band edge of the aged titania can be estimated as 382 nm (3.25 eV) with weak absorption at 400–600 nm. It was found that the

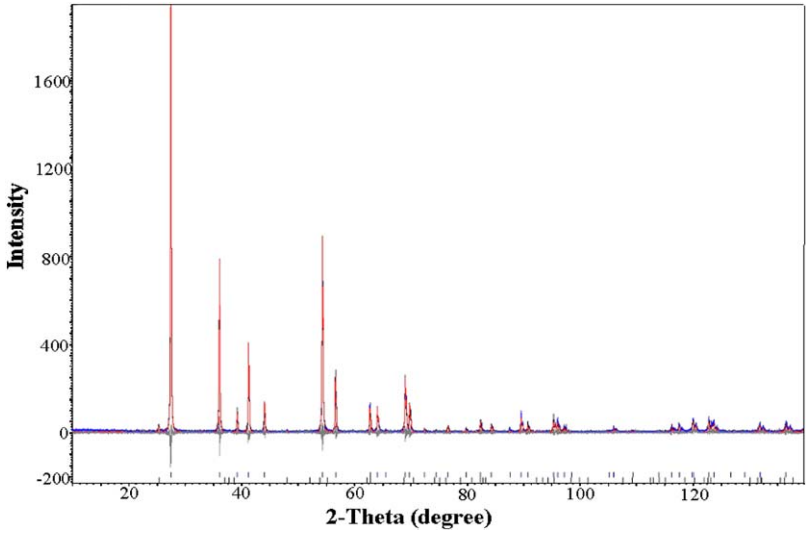

Fig. 5. Observed, calculated and difference profiles, resulting from the Rietveld analysis of X-ray powder diffraction data, for aged titania sample heat-treated at 700°C for 2 h.

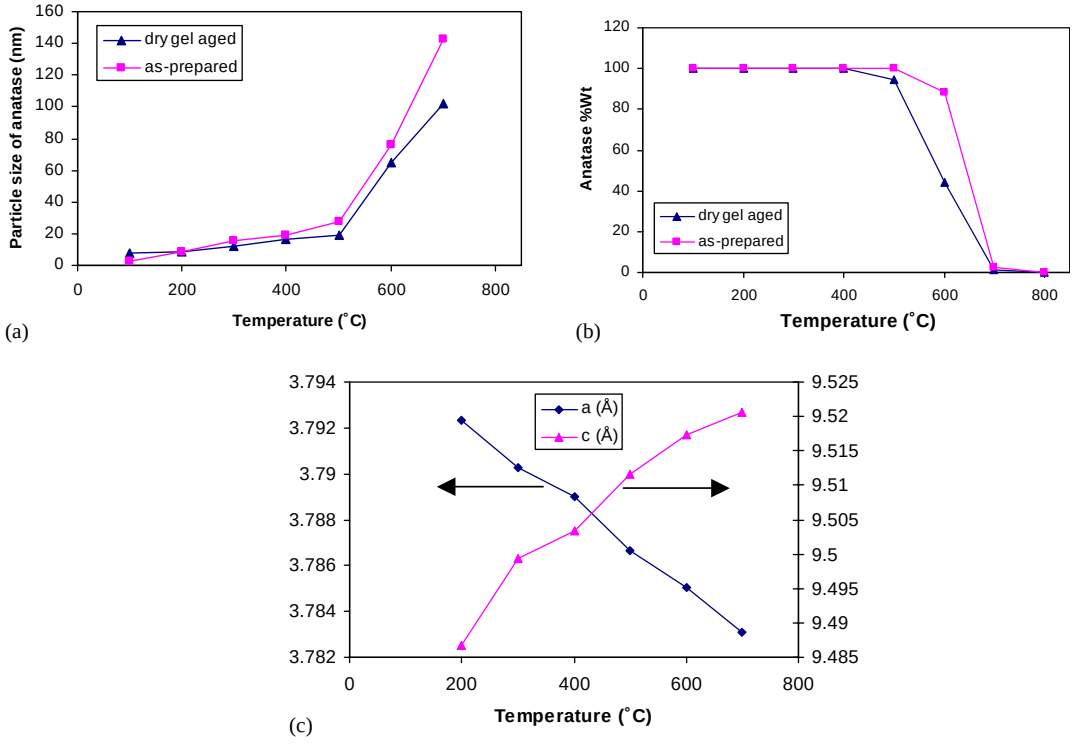

Fig. 6. XRD refinement results showing the phase development and unit cell trends during heat treatment.

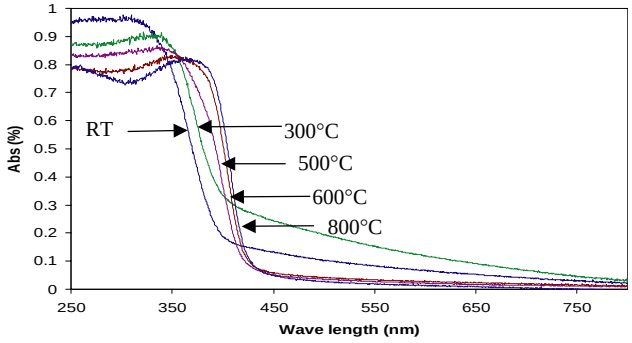

Fig. 7. UV–Vis spectra of aged titania nano-powders followed by heat-treatment at different temperatures for 2 h.

titania heat-treated at 800°C exhibited an absorption band edge at 414 nm (ca. 3.0 eV). The UV-absorption spectra show that absorption shifts to longer wavelength with increasing sintering temperature. At sintering temperatures <500°C, it is clear that size quantization causes the absorption edge to shift to lower energies. Above 500°C, the quantum size effect faded, and coincidentally the amount of rutile was higher. As the band gap of rutile (3.0 eV) is smaller than anatase (3.2 eV), the shift of the absorption edge to longer wavelengths would be expected.

The fact that titania powders aged at 100°C exhibit weak absorption at 400–600 nm at lower temperatures can be explained by the presence of surface groups formed during aging at 100°C, which form surface states [28,29]. The distorted surface components formed a surface state energy band that could lead to absorption at longer wavelengths. Our previous FTIR results show the existence of carbonates from 300°C to 400°C, which also supports this deduction [19].

3.2. *Effects of other processing parameters*

From the foregoing description, it is clear that aging of the dry gel promoted the crystallinity of anatase significantly and changed polymorph stability. Based on these results, the effect of wet gel aging and hydrolysis water ratio were studied.

3.2.1. *Aging time*

After gelation, the wet gels were stored at room temperature for up to 4 weeks prior to drying. The XRD patterns of the dry gels clearly demonstrated that longer aging times leads to greater crystallinity (Fig. 8). After 1 week, the intensities of peaks corresponding to anatase increased compared to the as-prepared titania (Fig. 3), while 3 weeks promoted the formation of rutile at room temperature. Peaks for rutile become more prominent after 4 weeks aging, indicating that aging of the wet gel favors the formation of this thermodynamically stable phase. In addition, the onset temperature for $A \rightarrow R$ transformation decreased nearly 600°C compared to the non-aged sample.

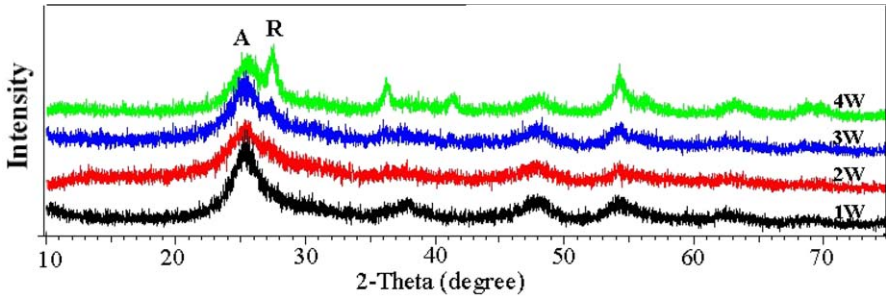

Fig. 8. XRD patterns of the titania dry gels at different gelation time.

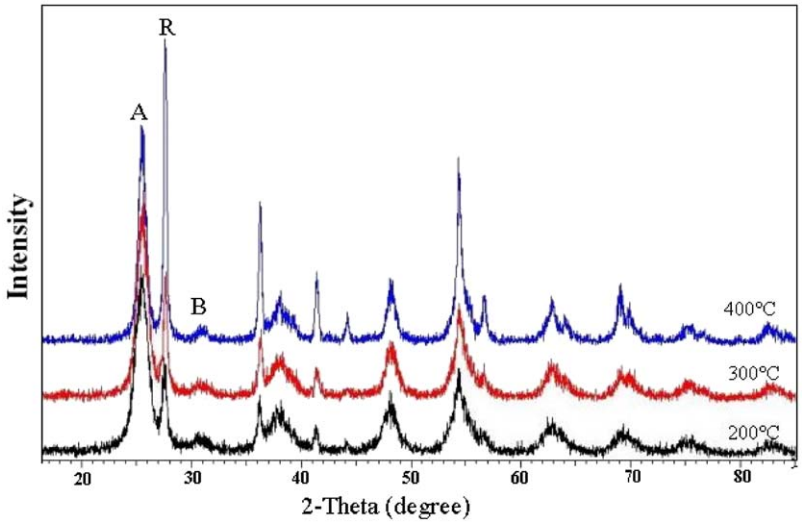

Fig. 9. XRD patterns of the titania powder with wet gel aged for 3 weeks.

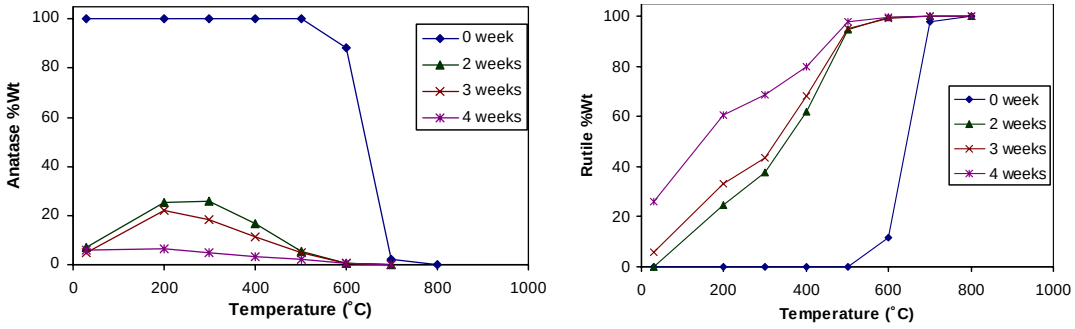

Fig. 10. Anatase and rutile phase development during sintering after aging the wet gel up to 4 weeks.

It is also noted that brookite appeared during aging the wet gel. Fig. 9 gives the XRD patterns of gels aged for 3 weeks followed by firing at 200–400°C. Brookite was only found in the temperature range of RT-400°C. The particle size of brookite was <10 nm before it transformed into anatase and rutile. The phase development during further heat treatment is shown in Fig. 10. The proportion of anatase in gels aged for 2 and 3 weeks increased at lower temperatures, while the amount of brookite decreased until it disappeared above 400°C. The weight percentage of rutile grew steadily during sintering in all of the aged samples, indicating that aging the wet gel promoted the formation of rutile, but its particle size was much smaller in the aged samples. According to the XRD refinement, rutile derived from aged gel has an average particle size of 110 nm compared to the 205 nm in the non-aged sample at 700°C after 2 h sintering.

Distinct morphologies were also evident at different sintering temperatures. Fig. 11 illustrates the morphological development in the sintered samples after aging the wet gel for 4 weeks. At lower temperatures, two

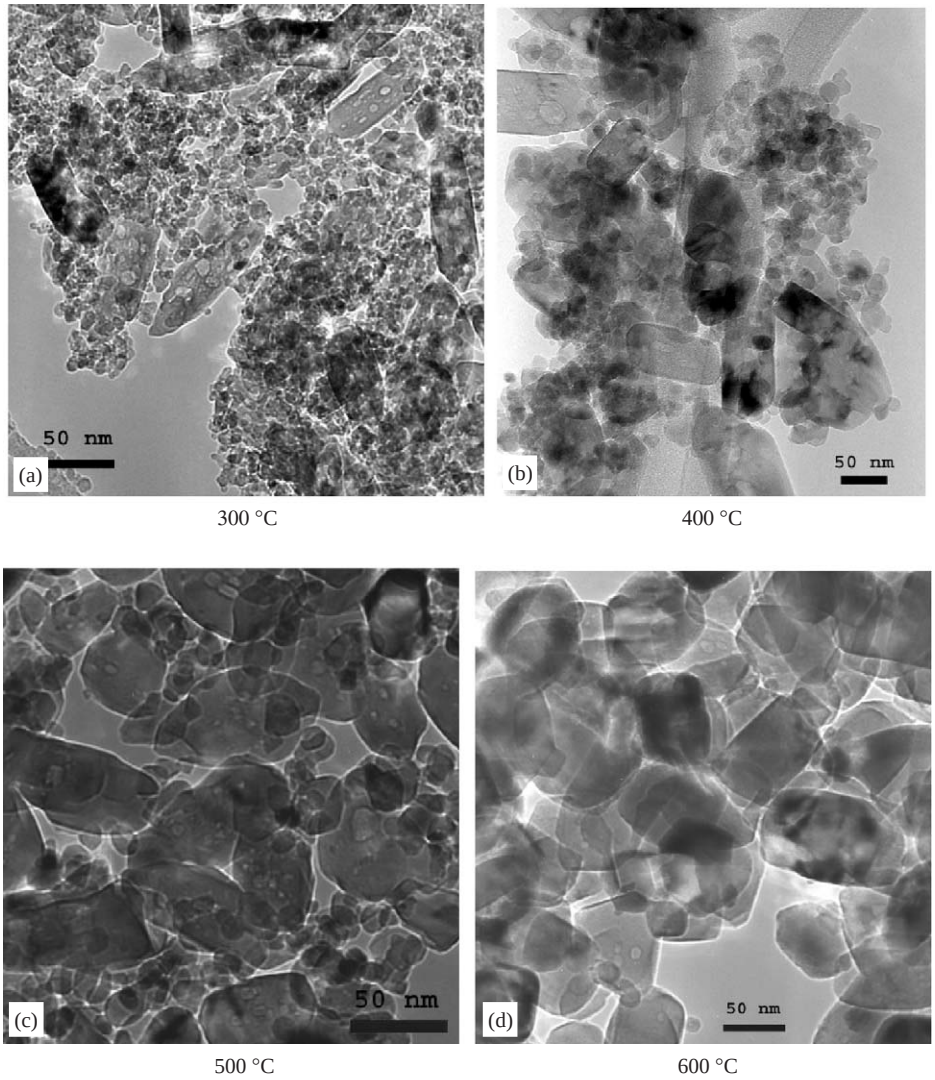

Fig. 11. TEM bright field images of titania powders heat treated at different temperatures for 2 h.

kinds of grain shapes, finely faceted particles and large lath-like grains could be recognized. The number of lath-like particles increased with increasing temperature. Detailed TEM analysis on different samples concluded that the fine facet particles are anatase and/or brookite, while the lath-like grains were rutile. The experimental and simulated SAED pattern and HRTEM image of the rutile from titania aged for 4 weeks followed by heat treatment at 500°C for 2 h is shown in Fig. 12.

3.3. Water concentration

The hydrolysis and polycondensation reactions of $Ti(O–Bu)_4$ were conducted at room temperature using four different water contents. The hydrolysis molar ratio ($r = [H_2O]/[Ti\ (O–Bu)_4]$) was changed in the range of 1, 2, 4 and 8, and the samples were labeled according to their hydrolysis water ratios, i.e., $1H_2O$–$8H_2O$.

The most important consequence is that gelation time is reduced significantly by increasing the water concentration as an increase in r accelerates the cross-linking process and reduces the gelation time [30]. At the highest water concentration ($r = 8$), some liquid is formed after gelation, as the hydrolysis ratio is high, macromolecular networks form rapidly through the reactions of hydrolysis and condensation, and have low interconnectivity. Consequently the network is rather loose, and the solvent may easily migrate out of the network. In contrast, a system with lower r will form slowly leading to a denser and more structured network that can incorporate a higher solvent concentration.

The gel powders synthesized from different water concentrations were calcined at various temperatures up to 700°C. For these samples, it was found that the weight percent and particle size of rutile (Fig. 13) were quite distinct at calcination temperatures >300°C. Specifically, the onset temperature of $A \rightarrow R$ decreased

with increasing r, this temperature difference between the $1H_2O$ and $8H_2O$ samples being 200°C. In addition, the rutile fraction was influenced by the water concentration. For the concentration chosen as $r = 8$, almost 98% of anatase phase has been transformed into rutile at 600°C after 2 h, but for the samples with $r = 1$ only 12% of anatase was transformed. Moreover, although rutile was formed at lower temperatures with increasing r, the particle size of rutile decreased, while that of anatase in different samples were similar.

4. Discussion

4.1. Precipitation mechanism

When alkoxide [Ti(OR)$_4$] reacts with water, the metal ion increases its co-ordination to six by using its vacant d-orbitals to accept oxygen lone pairs from nucleophilic ligands. These six-fold structural units undergo condensation and become the octahedra that are incorporated into the final precipitate structure [31]. The octahedra agglomerate through corner and/or edge sharing during the condensation reactions. Although the precipitates appear amorphous by X-ray diffraction, the existence of short range order similar to that in anatase [32] or brookite [33] have been confirmed by small angle X-ray diffraction.

When the initial reaction product of alkoxide and water is heated or aged at RT, crystalline precipitates are formed. The predilection for a particular polymorph to crystallize has been considered by several models. Henry et al. [34] described a possible pathway for the nucleation and growth of the rutile and anatase structure from aqueous solutions based on the Partial Charge Model. If deoxalation (O=Ti–OH_2→OH–Ti–OH) occurs before nucleation, condensation may be oriented towards *cis*-skewed chains characteristic of the anatase structure. If deoxolation occurs after nucleation, the *trans*-linear chain characteristic of the rutile structure is rather formed. Gopal et al. [35] pointed out that when the two octahedra join along an edge after initially sharing a corner during condensation, the placement of the third octahedron determines whether a rutile or an anatase/brookite nucleus is formed. If the third octahedron bonds to the two-octahedron to form a chain which is the basic structural unit of rutile, a nucleus favoring this polymorph is produced. If the third octahedron joins in such a way that a right angle is formed (the basic structural unit of anatase/brookite), anatase and/or brookite may appear. The rutile configuration is thermodynamically favorable because its linearity allows the relaxation of Ti–Ti bond, leading to lower nucleation activation energy. In contrast, the right-angle configuration cannot relax as easily, but statistically favors nucleation of anatase/brookite.

Based on the above discussion, it may be thought that in one liquid system there may exist several kinds of growth units. The competition between the different growth units of rutile and anatase/brookite and the relative stabilities (from the aspect of energy and

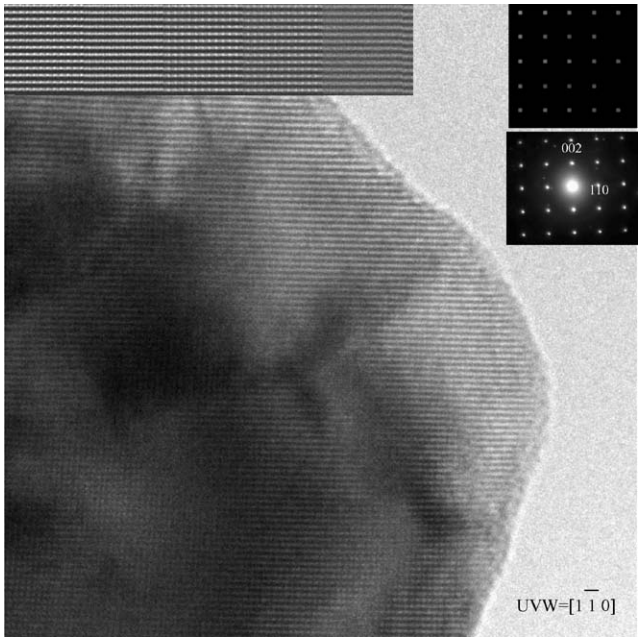

Fig. 12. SAEDP and HRTEM image of the titania powders with 4 weeks aging time.

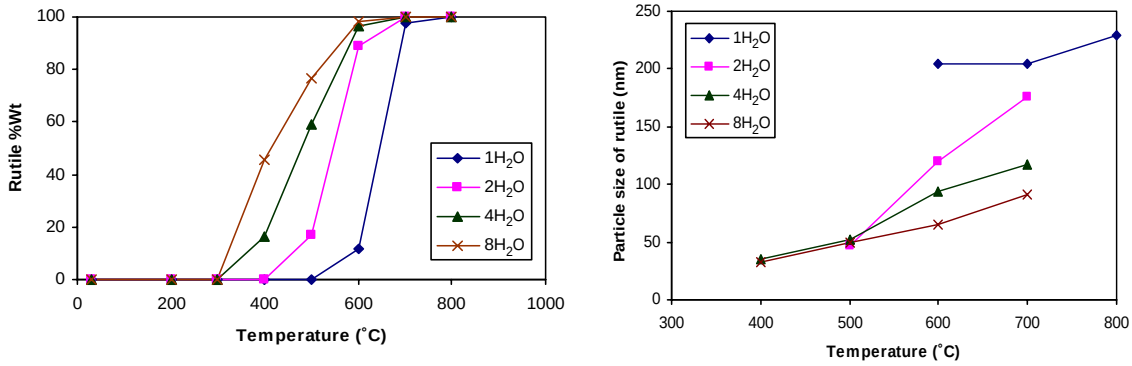

Fig. 13. Temperature dependence of percentage and particle size of rutile in the samples with different water concentration.

geometric configuration) depend on the processing parameters. The probability for the formation of the specific polymorph will be proportional to the number and type of growth units. Bosc et al. [36] assigned the structure of the dispersed alkoxide-derived colloids to anatase after aging for 3 h, while the precipitate obtained for longer aging (>5 h) corresponds to a mixture of anatase and rutile. Yin et al. [37] concluded that chelation of TiO_6 octahedra with citric acid and acidification with nitric acid are critical for the phase transition from amorphous to rutile. In this study, aging of the dry gel at 100°C for 12 h favored the growth of anatase nuclei, and improved its crystallinity. The particle size of anatase can be controlled by adjusting the dry gel aging time. Aging of the wet gel at room temperature also promotes the crystal growth of anatase and brookite at the initial stage. Keeping the wet gel for longer periods favors the formation of rutile. The amount of rutile can be controlled by adjusting the wet gel aging time.

4.2. Polymorph transformations

The transformation sequence among anatase, brookite and rutile depends on their initial particle size, as this determines the thermodynamic stability of the polymorphs at ultra-fine sizes. In their experiments, Zhang and Banfield [38] found that at a particle size less than 11 nm, anatase was the most stable phase; between 11 and 35 nm, brookite was favored; while above 35 nm, rutile was preferred. In this study, particle size was not the only factor influencing the $A \rightarrow R$ transformation. It is also clear that both aging the dry gel and higher r lower the $A \rightarrow R$ onset temperature. The particle sizes of anatase before $A \rightarrow R$ are quite similar, and larger than the critical particle size calculated by other researchers (14–16 nm). The transformation of anatase to rutile is reconstructive, and is governed by interface nucleation and/or surface nucleation [39]. Aging the dry gel may change the surface/interface structure, making the nucleation of rutile possible at lower temperatures. In the sol–gel process, the amount of water determines the degree of hydrolysis and the type of initial species formed, thus influencing the secondary polycondensation reactions which involve the polymerization of hydrolyzed metal alkoxides in alcoholic solution. This in turn affects the surface structure of the resultant titania powders, and may be responsible for the decrease in the $A \rightarrow R$ onset temperature.

In the as-prepared and aged dry gel samples, anatase remains as the only phase at lower temperatures and its particle growth is slow between 200°C and 400°C. However, for temperatures $\geqslant$500°C, the average particle sizes of anatase are smaller than that of the as-prepared samples with heat treatment at the same temperatures (Fig. 6(a)). It is noteworthy that in the aged dry gel, anatase commenced transformation to rutile at 500°C, which is 100°C lower than for the as-prepared sample. Those anatase particles larger than a certain value would transform to rutile, leading to a reduction in the average particle size of the remaining anatase.

Another common phenomenon to be noticed is that the lower the $A \rightarrow R$ onset temperature, the smaller the rutile particle size when heat treated at same temperature (see Fig. 13). This is because at low temperature, the net transformation rate is limited by the rate of rutile nucleation rather than rutile growth. Parameters favoring rutile formation must provide more sites for rutile nucleation. The more the nuclei of rutile, the smaller the particle sizes.

Brookite was only formed in the samples aged as wet gels. During calcination, both the amount of anatase and brookite increased initially, and then both decreased as the percentage of rutile increased above 300°C (Fig. 10). These results indicate that brookite may transform to anatase and/or rutile, and then anatase transforms to rutile.

According to Penn and Banfield [40], the interconversion of anatase and brookite involves minor displacements of some atoms into adjacent sites. Thus the activation energy for the $B \rightarrow A$ transformation should be much lower than that for the $B \rightarrow R$ transformation. Only those brookite particles whose diameters are larger than a certain value can transform to rutile. If the particle size is less than that value, brookite is more thermodynamically stable than rutile at lower temperatures. The remaining brookite has a particle size less than 10 nm below 400°C, and above that temperature, brookite disappeared.

5. Conclusions

The influence of preparation parameters on the microstructure and thermostability of titania powders was studied systematically. It is concluded that preparative methods substantially determine the crystal structure of the nanocrystalline titania. The particle size of anatase can be controlled by adjusting the aging time of the dry gel. The amount of rutile can be controlled by adjusting the wet gel aging time.

Particle size is not the only factor to influence the transformation between nano-sized anatase and rutile. The surface structure also contributes to the nucleation of rutile and hence the $A \rightarrow R$ conversion. Brookite transforms to anatase and/or rutile at lower temperatures, and then anatase transforms to rutile.

Acknowledgments

This work was supported through ASTAR Grant 012 105 0123. Valuable discussions with Dr. Zhili Dong and

Dr. Cristiano Ferraris are gratefully acknowledged. The authors would like to thank Dr. Ken Chiang, Mr. Leslie Tsen, Mr. Terence Chin, Ms. Ng Yuen Ling for their assistance with the UV–Vis spectrophotometer, BET surface analysis, DSC/TGA and FTIR spectrometer experiments.

References

[1] N.I. Al-Salim, S.A. Bagshaw, A. Bittar, T. Kemmitt, A.J. McQuillan, A.M. Mills, M.J. Ryan, J. Mater. Chem. 10 (2000) 2358–2363.
[2] S. Ito, S. Inoue, H. Kawada, M. Hara, M. Iwaski, H. Tada, J. Colloid Interface Sci. 216 (1999) 59–64.
[3] X.Z. Ding, X.H. Liu, Mater. Sci. Eng. A 224 (1997) 210–215.
[4] J. Moon, H. Takagi, Y. Fujishiro, M. Awano, J. Mater. Sci. 36 (2001) 949–955.
[5] J. Ovenstone, J. Mater. Sci. 36 (2001) 1325–1329.
[6] R.C. Weast (Ed.), Handbook of Chemistry and Physics, CRC Press, Boca Raton, FL, B-154, 1984.
[7] J.A. Montoya, P. Angel, T. Viveros, J. Mater. Chem. 11 (2001) 944–950.
[8] M.P. Coles, C.G. Lugmair, K.W. Terry, D. Tilley, Chem. Mater. 12 (2000) 122–131.
[9] M. Kallala, C. Sanchez, B. Cabane, J. Non-Cryst. Solids 147–148 (1992) 189–193.
[10] C.U.I. Zoulin, J. Mater. Sci. Techol. 15 (1999) 71–74.
[11] G. Oskam, A. Nellore, R.L. Penn, P.C. Searson, J. Phys. Chem. 107 (2003) 1734–1738.
[12] J.C. Yu, J. Yu, L. Zhang, W. Ho, J. Photochem. Photobiol. A 148 (2002) 263–271.
[13] B.-R. Li, X.-H. Wang, M.-Y. Yan, L.-T. Li, Mater. Chem. Phys. 78 (2002) 184–188.
[14] D. Vorkapic, T.J. Matsoukas, J. Colloid Interface Sci. 214 (1999) 283–291.
[15] C.J. Barbé, F. Arendse, P. Comte, M. Jirousek, F. Lenzmann, V. Shklover, M. Grätzel, J. Am. Ceram. Soc. 80 (1997) 3157–3171.
[16] A. Fujishima, T.N. Rao, D.A. Tryk, J. Photochem. Photobiol. C: Photochem. Rev. 1 (2000) 1–21.
[17] X. Liu, J. Yang, L. Wang, X. Yang, L. Lu, X. Wang, Mater. Sci. Eng. A 289 (2000) 241–245.
[18] I. Zhitomirsky, J. Eur. Ceram. Soc. 19 (1999) 2581–2587.
[19] Y. Li, S.H. Lim, T. White, Mater. Trans. 44 (2003) 1328–1332.
[20] TOPAS, User's Manual, Bruker Advanced X-ray Solutions, Bruker AXS GMBH, Karlsruhe, Germany, 2001.
[21] K.I. Gnanasekar, V. Subramanian, J. Robinson, J.C. Jiang, F.E. Posey, B. Rambabu, J. Mater. Res. 17 (2002) 1507–1512.
[22] C.J. Barbe, F. Arendse, P. Comte, M. Jirousek, F. Lenzmann, V. Shklover, M. Gratzel, J. Am. Ceram. Soc. 80 (1997) 3157–3171.
[23] Q. Xu, M.A. Anderson, J. Mater. Res. 6 (1991) 1073–1081.
[24] K. Suglyama, Y. Takeuchi, Z. Kristallogr. 194 (1991) 305–313.
[25] E.P. Meagher, G.A. Lager, Can. Mineral. 17 (1979) 77–85.
[26] C.J. Howard, T.M. Sabine, F. Dickson, Acta Crystallogr. 47 (1991) 462–468.
[27] M. Anpo, T. Shima, S. Kodama, Y. Kobokawa, J. Phys. Chem. 91 (1987) 4305–4310.
[28] Y.-C. Zhu, C.-X. Ding, J. Solid State Chem. 145 (1999) 711–715.
[29] P. Salvador, C. Gutierrez, J. Electrochem. Soc. 131 (1984) 326–336.
[30] A. Ponton, S. Barboux-Doneuff, C. Sanchez, Colloids Surf. A 162 (1999) 177–192.
[31] J. Livage, M. Henry, C. Sanchez, Prog. Solid State Chem. 18 (1988) 259–341.
[32] J.R. Bartlett, J.L. Woolfrey, in: L.L. Hench, J.K. West (Eds.), Chemical Processing of Advanced Materials, John Wiley, New York, 1992, p. 247.
[33] Q.J. Wang, S.C. Moss, M.L. Shalz, A.M. Glaeser, H.W. Zandbergen, P. Zschack, in: P. Jena, S.N. Khanna, B.K. Rao (Eds.), Physics and Chemistry of Finite Systems: from Cluster to Crystals, Vol. II, Kluwer Academic Publishers, Boston, 1992, p. 1287.
[34] M. Henry, J.P. Jolivet, J. Livage, Struct. Bond. 77 (1992) 155–206.
[35] M. Gopal, W.J. Moberly Chan, L.C. De Jonghe, J. Mater. Sci. 32 (1997) 6001–6008.
[36] F. Bosc, A. Ayral, P.-A. Albouy, C. Guizard, Chem. Mater. 15 (2003) 2463–2468.
[37] H. Yin, Y. Wada, T. Kitamura, S. Kambe, S. Murasawa, H. Mori, T. Sakata, S. Yanagida, J. Mater. Chem. 11 (2001) 1694–1703.
[38] H. Zhang, J.F. Banfield, J. Phys. Chem. B 104 (2000) 3481–3487.
[39] H. Zhang, J.F. Banfield, J. Mater. Res. 15 (2000) 437–448.
[40] R.L. Penn, J.F. Banfield, Am. Mineral. 83 (1998) 1077–1082.